1 *Article*

2 # Influence of Nanoscaled Surface Modification on the
3 # Reaction of Al/Ni Multilayers

4 **Heike Bartsch [1,*], José Manuel Mánuel [2,3] and Rolf Grieseler [1,4]**

5 [1] Technische Universität Ilmenau, Institute for Micro- and Nanotechnologies, MacroNano®, 98693 Ilmenau,
6   Germany; heike.bartsch@tu-ilmenau.de
7 [2] Universidad de Cádiz, Facultad de Ciencias, 11510 Puerto Real, Spain; jose.manuel@uca.es
8 [3] IMEYMAT: Institute of Research on Electron Microscopy and Materials of the University of Cádiz, Spain.
9 [4] Pontificia Universidad Católica del Perú, San Miguel-32 Lima
10 * Correspondence: heike.bartsch@tu-ilmenau.de; Phone: +49-3677-69-3452

11 **Abstract:** Sputtered reactive multilayers applied as a heat source in electronic joining processes are
12 an emerging technology. Their use promises low-stress assembly of components while improving
13 the thermal contact and reducing the thermal resistance. Nanostructured surface modifications can
14 significantly enhance adhesion and reliability of joints between different materials. This work
15 examines reactive multilayer of nickel and aluminum, directly sputtered on nanostructured black
16 silicon surfaces and compares their phase transformation with reference samples deposited on
17 pristine silicon surface. The investigation of the quenched self-propagating reaction reveals a clear
18 influence of the nanostructured surface on the prolongation of the phase transition. Rapid thermal
19 annealing tests result in the formation of $Al_{1.1}Ni_{0.9}$ phase. The nanostructured interface seems to
20 hinder the full transformation of the parent material. The surface modification improves the
21 adhesion of the formed alloy on silicon surfaces and can possibly increase the reliability of joints
22 based on reactive aluminum/nickel multilayer. The use of black silicon, a nanostructured surface
23 modification, is thus a promising approach to realize reliable multi-material joints in complex
24 systems.

25 **Keywords:** reactive multilayer; sputtering; self-propagating reaction; aluminum/nickel; black
26 silicon; joining technology; nanostructured silicon; reactive nanomaterial
27

28 **1. Introduction**

29   Today's electronic systems must provide increased performance whilst reducing size at the same
30 time. This pushes the development of effective and cost-efficient methods of heat removal [1]. Overall
31 thermal challenges encompass hot spot thermal management on packaging level and heat spreading
32 from chip to heat sinks [2]. This entails enhanced requirements on thermal interface materials [3]. The
33 direct mount of chips on heat sinks, strongly driven by packaging requirements of LED chips, enters
34 the field of integrated circuit and MEMS packaging. However, the assembly of complex dies with
35 numerous contacts and fine pitch makes high demands and the huge mismatch of thermal expansion
36 between silicon and heat sink must be compensated in order to minimize stress.
37   One solution for stress minimization is the use of local heat exposure during the bond process
38 [4]. Self-propagating exothermic reactions of multilayer films can be used to generate a local heat
39 source and melt a solder between silicon chips and board or heat sink. The reaction is driven by a
40 reduction in atomic binding energy. The mechanism is observed when multilayer films of bimetal
41 layers with a single layer thickness between 10 nm and 150 nm, such as Ni/Si, Al/Ti, Al/Ni or Al/Pd,
42 are ignited with an energy pulse, e.g. an electric spark or a laser pulse.
43   Several works dwell on the use of such reactive multilayers (RML) for chip joining. One
44 approach uses aluminum nickel nanofoils in combination with Indium solder. A thermal interface
45 with improved performance in comparison with polymeric-based ones is created at room
46 temperature. Due to a very restricted heating zone, the thermal stress is minimized and a tight bond

47   is achieved [5]. The direct deposition of reactive layers on components expands the material variety
48   and allows improved stress control. Sputtered Ti/Si and Al/Pd multilayers form bond interfaces using
49   Sn solder for the assembly of silicon MEMS at room temperature [6]. These integrated RML allow the
50   direct and hermetic bond between two silicon chips and between silicon and ceramic, glass and metal
51   as well [7]. Al/Ni integrated RML, directly deposited on LTCC ceramic can be used for the joining of
52   copper heat sinks. The higher roughness of the ceramic substrate leads to a better adhesion in
53   comparison with pristine wafer surfaces [8]. Al/Ni RML stand out through a very fast exothermic
54   propagation, easy preparation and easy ignition. However, stress control is an ongoing topic using
55   these materials in order to avoid cracks and voids, which reduce thermal performance [9]. Beside of
56   thermal performance increase, improved mechanical compliance is an ongoing target in the
57   development of TIMs. Metallic interlayer can be used to increase the strength, because the type of
58   interlayer influences the fracture origin [10]. A further approach a stress reduction is the use of
59   nanostructured interfaces. Nanothermal interfaces can reach very low thermal resistance,
60   undercutting values of 1 W/m^{-1}K^{-1} [11]. An enhancement of the bonding strength can be achieved by
61   surface modifications of silicon in the nanoscale. Surface enlargement and additional form fit affect
62   adhesive bond strength and ductility of the interface [12], [13]. Plasma etching of the silicon surface
63   generates nanostructures by self-masking, the so-called black silicon [14]. The cost-effective process
64   can be easily applied on any silicon surface in plasma processes used for mesa-structure etching of
65   chips. If this surface modification entails a stress reduction in combination with RML chip assembly,
66   the chip would be optimally prepared and additional process steps such as sputtering of intermediate
67   layers can be omitted. With this motivation, the present work aims to give a first insight into the
68   interplay between surface morphology and reaction behavior of Al/Ni RML. A comparison between
69   pristine silicon wafer surface and black silicon modified one, sputtered with aluminum/nickel as
70   parent multilayer is base of the discussion focusing on parent multilayer growth, reactive multilayer
71   thickness and their influences on phase forming and reaction propagation. On this base, a scenario
72   for possible applications of RML on black silicon as nanothermal interface for chip mounting is
73   outlined.

74   **2. Materials and Methods**

75   Black silicon is formed as a consequence of self-organized micromasking in fluorine based
76   reactive ion etch processes of silicon wafers [14]. The geometry of the needles depends on the etch
77   process [15]. In this work, nanostructure etching is performed in an Oxford RIE reactor with a
78   pressure of 100 mTorr, working at a power of 100 W and 20°C with helium backing, using a gas flow
79   of 84 sccm SF$_6$, and 66 sccm O$_2$. P-doped (111) silicon wafer are used as substrate. The process was
80   maintained during 30 minutes, resulting in needles of approximately 1.0 µm of length. A pristine, flat
81   wafer without nanostructures is used for comparison purpose. On both substrate types, the
82   nanostructured silicon wafer and the flat ones, aluminum/nickel RML are directly applied. The layer
83   consists of alternating nanoscaled single layers of pure aluminum and nickel which were deposited
84   by magnetron sputtering. The bilayer thickness amounts to 50 nm. The process was carried out using
85   a cluster system (CS400 by ARDENNE) with a sputtering power of 200 W and a working pressure of
86   5·10^{-3} mbar with 80 sccm argon flow and without substrate heating. The obtained deposition rate was
87   0.32 nm/s for aluminum and 0.26 nm/s for nickel. The total thickness of the multilayer sequence varies
88   between 250 nm and 5 µm. The experimental design is summarized in Table 1.

Table 1. Overview on samples and experimental design.

No	Substrate	Bilayer thickness [nm]	Total RML thickness [nm]	RTA Tmax [°C]	Spark ignition [V] / [mA]
1	Flat wafer	50	1000	350 / 450 / 550	-
2	Flat wafer	50	5000	350 / 450 / 550	50 / 50
3	Black silicon	50	500	350 / 450 / 550	50 / 50
4	Black silicon	50	1000	350 / 450 / 550	50 / 50
5	Black silicon	50	5000	350 / 450 / 550	50 / 50

89   The prepared wafers are mechanically carved along the substrates main crystallographic
90   directions using a diamond tip and broken in samples with an edge length between 1 and 2 cm. One
91   piece of each wafer was stored for reference, one was ignited by electric spark and three pieces were
92   annealed at different temperature. The layer morphology on the nanostructures was investigated by
93   SEM (Field-Effect ZEISS Gemini SEM 500 working at 1.5 kV and working distance of 8 mm) and TEM
94   (TECNAI S20 working at 200 kV). SEM micrographs were obtained by positioning the broken pieces
95   of the samples, without further preparation, in a planar or a transversal disposition regarding to the
96   electron beam. TEM preparation consisted in scratching the nanostructured and coated surface of the
97   samples with a surgical blade, in order to separate the needles from the silicon substrate. The
98   separated needles were deposited on holey-carbon grids without further preparation for the TEM
99   measurements. The images of SEM and TEM analysis are depicted in Figure 1. Self-propagating
100 reactions were initiated on one sample of each wafer. An electric spark was formed between a
101 platinum electrode and the coated surface, applying a voltage of 50 V and a maximum current of
102 50 mA with a lab power supply. 50 ignition points were generated and their dimensions were
103 investigated with a light microscope in order to assess the influenced region dependent on multilayer
104 thickness on an adequate confidence level. The influenced region can be identified by a color change
105 with a light microscope. The affected area of the nanostructured samples and the 5 μm thick flat
106 sample was investigated with a light microscope (Nikon Eclipse LV100POL) and the radius of the
107 affected spots was measured with the microscopes image processing software (NIS Elements Imaging
108 Software 4.30.00, Nikon). The discolored area is enclosed with a circle, defined on three points on the
109 circumference, the software calculates the affected radius r_{aff} and the values are summarized in an
110 Exel-sheet. The box plots in Figure 2 a display median and quantiles of the respective value
111 distribution on nanostructured samples. The morphology of the affected zone was investigated by
112 SEM (Field-Effect ZEISS Gemini SEM 500 working at 1.5 kV and working distance 8mm). Fused areas
113 were subsequently colored in purple to achieve a better visibility. Selected pictures are depicted in
114 Figure 2 (b-e).

115   Further, samples of each wafer were annealed in a rapid thermal furnace (Jet First, Joint
116 Industrial Processor for Electronics) under argon atmosphere (RTA). The maximum temperature T_{max}
117 was varied between 350°C and 550°C. Figure 3 a) illustrates temperature treatment and gas flow
118 regime, 3 b) gives a schematic of the reactor setup. Treated and untreated samples were investigated
119 with a laser scanning microscope (LSM, Olympus OLS4100), selected surface pictures and a height
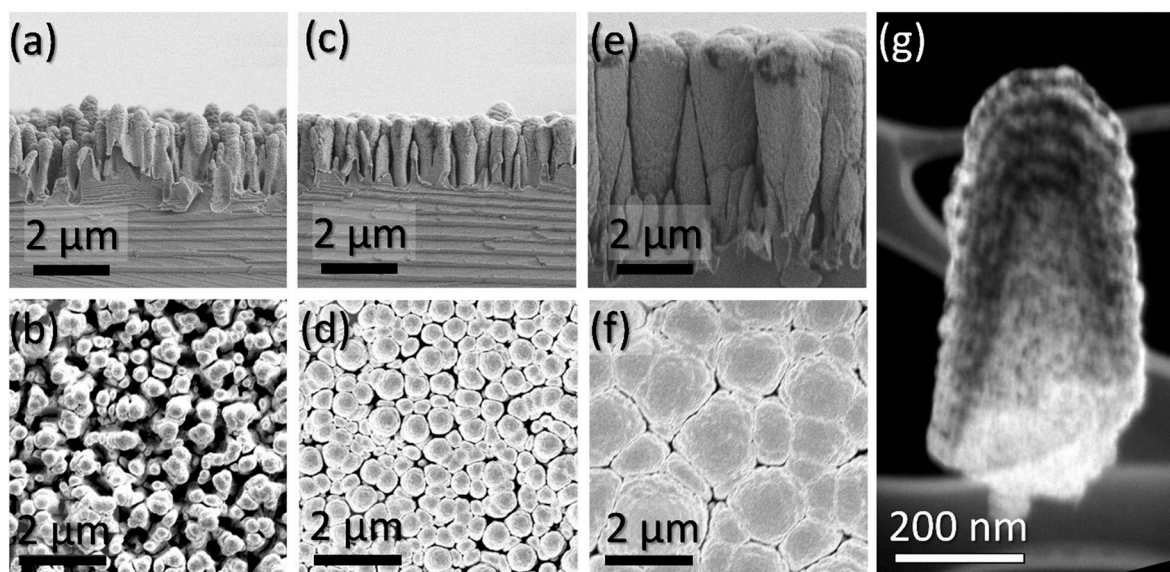
Figure 1. SEM micrographs of multilayers with different thickness, grown on black silicon
nanostructures: a), c), e) cross section of thick multilayers with 500 nm, 1 μm and 5 μm thickness;
b), d), f) top view on the respective layer; g) Dark Field TEM image of a nanostructure tip with 20
nm radius, coated with a 250-nm-thick multilayer.
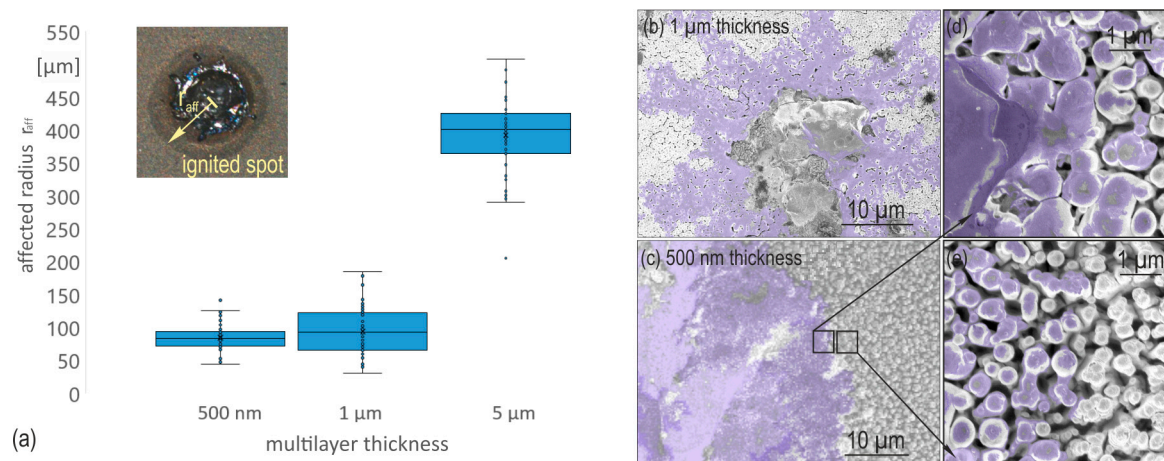
Figure 2. Affected zone dependent on layer thickness on nanostructured surface. (a) box plot of the affected radius measured by light microscope as function of layer thickness; (b) false color SEM image of ignition zone; zone is minimal larger and has dendrite shape, form is irregular, fractal distribution of the ignition over nanostructures on top, molten areas are colored (c) false color SEM image of 500 nm layer. Ignited zone has a round shape, molten area ends abruptly (d) detail of the border area, molten layers on top are depicted in false color (e) outermost area of influenced zone, some tips show fused structure (false color).

120 profile are compared in Figure 4. The treated samples were investigated with XRD (Bruker D5000
121 diffractometer with Göbel mirror, working in Bragg-Brentano mode at a speed of 0.1 seconds per
122 step, using sampling steps of 0.04° without sample rotation) to identify formed phase and grade of
123 phase formation. Diffractograms were recorded over the 20°<2θ<100° range. Phase identification was
124 performed by analyzing the positions and intensities of the peaks observed in the diffractograms and
125 comparing them with data bases patterns. Extracts between 20° and 65° are depicted in Figure 5.
126 Energy dispersive X-ray spectroscopy (EDX) is carried out at 20 kV acceleration voltage (EDAX
127 detector with super ultra-thin window of 30 mm² area, nitrogen cooled) in order to determine the
128 chemical composition.

129 **3. Results**

130 *3.1 Parent multilayer morphology on nanostructures*

131   The parent bilayer layer consists of alternating sequences of fcc Ni and fcc Al, identified by
132 comparison of the XRD diffractograms with PDF 03-065-2865 and PDF 03-065-2869. EDX analysis
133 reveals a composition of 50 at % Ni : 50 at % Al with a deviation of 3%. The cross sections in Figure 1
134 a), c) and e) illustrate that the edge coverage of the sputtered layers on black silicon is not uniform.
135 A progressive growth of larger clusters at the structure top at the expense of smaller ones occurs.
136 With increasing thickness, the gaps between single nanostructures are filled from the top of the
137 substrate. While single structures covered with a 500-nm-thick multilayer still are separated, some
138 touch at the top when the layer is 1 μm thick. The black silicon structures covered with a 5-μm-thick
139 layer have direct contact on top, visible in the top view 2 b), d), f). However, the cross sections indicate
140 that hollows are present at deeper levels. The TEM image in Figure 1 g) reveals that the deposition
141 rate at the nanostructure´s foot is much lower than on top, resulting in a steady decrease of the bilayer
142 thickness. At a depth of approx. 500 nm from the top of the structure, the bilayer thickness is only ¼
143 of the one on the structure top. In all probability, the intermixed layer formed during sputtering and
144 pure metal layers reaches similar thickness at the structure foot, resulting in disruption of the crystal
145 structure, grain boundary structure and lattice structure in this region.
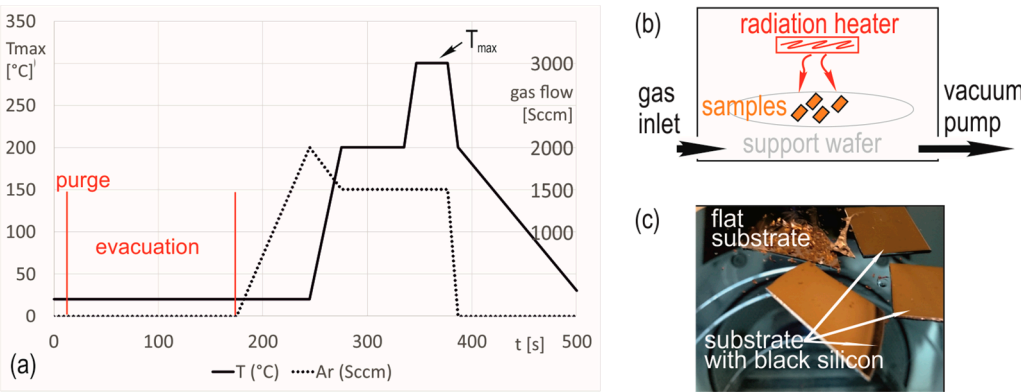
Figure 3. Rapid thermal annealing (RTA) process. (a) Temperature profile with gas flow regime, T_{max} varies between 350°C and 550°C, the heat-up time is 12 s and plateau time 30s; (b) Schematic of RTA set-up; (c) Photograph of treated samples on support wafer.
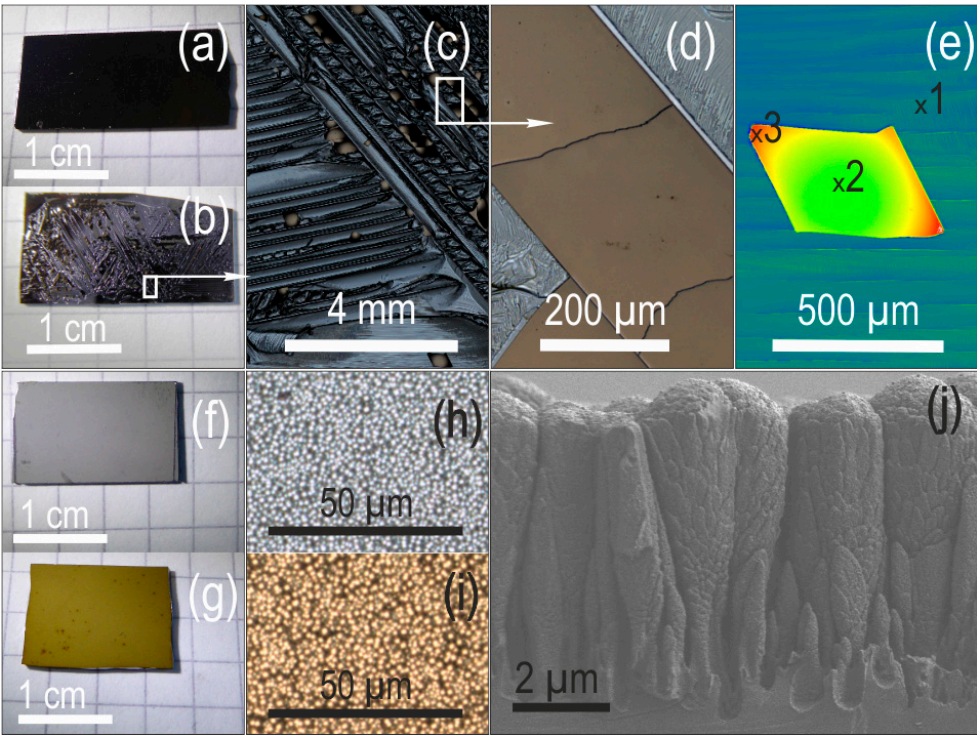
Figure 4. Comparison of RTA test samples before and after treatment at 450°C. (a-e) flat silicon chip; (a) before treatment; (b) after treatment; (c) LSM image of the surface after treatment; (d) LSM image of a transformed area; (e) Height map of an adhered flake. Height level at point 1 = 0 μm, point 2 = 28 μm, point 3 = 50 μm. (f-j) chips with black silicon; (f) chip with 1 μm RML before treatment; (g) after treatment; (h) LSM image of the chip surface, 5 μm RML before and (i) after treatment; (j) Cross-sectional SEM image of the transformed RML with 5 μm thickness.

3.2 Spark ignition

Molten ares are visible on all samples around the ignition point. This molten zone is surrounded with a ring, which can be recognized by a color change under the ligth microscope. The border of this region marks the end of the affected material and is used to asses the affected zone by spark ignition. The box plot of the affected zones radius r_{aff}, measured on black silicon for different Al/Ni multilayer thickness, is depicted in Figure 2 a). The values follow a Gaussian distribution. The dependency of the median values of r_{aff} on layer thickness can be approximated by a quadratic polynom with high
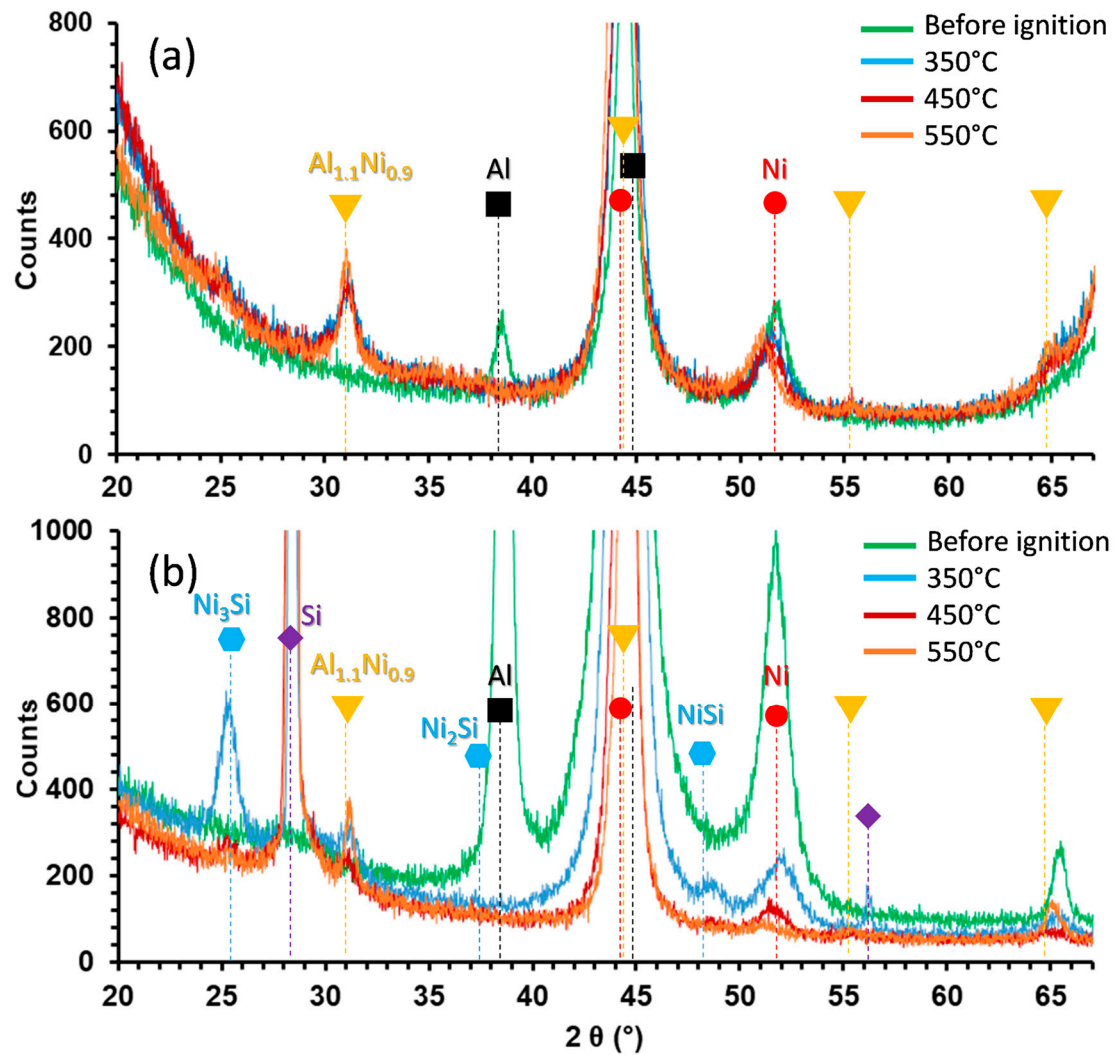
Figure 5. XRD Theta-2Theta curve of RTA treated samples with 1 μm RML thickens, (a) on black silicon surface; (b) reference on flat wafer. Identification peaks are associated to PDF 03-065-2869 (fm-3m Al), 03-065-2865 (fm-3m Ni) and 00-044-1187 (pm-3m $Al_{1.1}Ni_{0.9}$).

153   accuracy. Median values correspond to 84 μm for 500 nm Al/Ni multilayer thickness, 92 μm for 1 μm
154   and 391 μm for 5 μm. The comparison between r_{aff} of the 5-μm-thick flat sample, which amounts to
155   468 μm, and this of the nanostrutured interface with equal RML thickness shows that black silicon
156   surface modification narrows down the affected zone. R_{aff} is reduced to 80 percent. The shape of the
157   affected area on black silicon is depicted in Figure 2 b) and c). The influenced zone of 5 μm-thick-
158   layer (not depicted) and 500 nm thick layers are characterized by a round contour. The transition ring
159   area between molten material and unaffected structures has a width of 100 μm for 5-μm-thick layers.
160   In the case of 500-nm-thick layers it is restricted to 10 μm, approximately. Details of this transition
161   area are depicted in Figure 2 d and e). While the structures in the near vicinity still show closed
162   molten links to the spark area, those next to them are characterized by a changed morphology, but
163   not linked with adjacent ones. Ignited regions on samples with 1-μm-thick Al/Ni multilayers are
164   characterized by a dendrite shape of the molten areas. The reaction propagates along paths were the
165   tips of the nanostructures have contact and peters out. The affected area identified by light
166   microscope has mostly circular and in some cases eliptical contour.
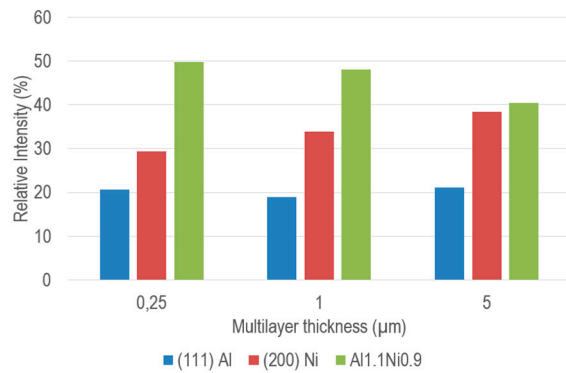
Figure 6. Relation between the intensities of selected peaks as marker for Al, Ni and Al$_{1.1}$Ni$_{0.9}$ content after RTA treatment at 350°C.
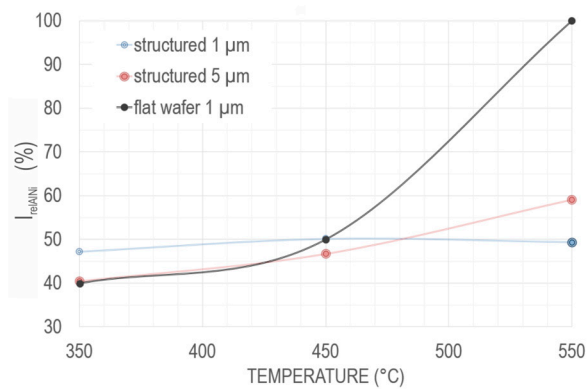
Figure 7. Relative intensity I$_{AlNi}$ for total thickness of 1 μm and 5 μm compared with 1-μm-thick layer on flat reference wafer.

3.3 Rapid thermal annealing

The RTA process uses heat radiation to initiate the phase transformation, which is here driven by solid diffusion. Layers on flat silicon surfaces (compare Figure 4 a) flake during the treatment, independently from thickness and maximum temperature. An example is depicted in 4 b-e). A remarkably orientation of chipped traces is visible in Figure 4 b). The peel-off seems to follow the single-crystal structure of the silicon substrate. Trapezoidal flakes are formed as depicted in Figure 4 c). These exhibit strong tensile stress, which can be concluded from the strong bend visible in Figure 4 e). Layers on black silicon showed excellent adhesion without exception. Photographs of samples with 1 μm coating before and after treatment at 450°C are depicted in Figure 4 f, g). Surface images captured with LSM are depicted in Figure 4 h, i). The phase transformation can optically be identified by the color change. Neither the LSM top view Figure 4 i) nor the cross-sectional SEM image Figure 4 j) exhibit signs of molten material.

XRD difractograms are depicted in Figure 5. The parent materials exist in form of fcc Al (PTC 03-065-2869) and fcc Ni (PTC 03-065-2865) before RTA. (111) Al peak at 2Θ = 38.471° and (200) Ni peak at 2Θ = 51.847° are clearly evident. Between 44°< 2Θ < 45°, both parent materials and possible formed Ai/Ni phases as well have peaks, for that reason these cannot contribute to analysis. After annealing, the (111) Al peaks disappear, and the AlNi phase peaks arise around 2Θ = 31.2° and 55.5°. Further peaks AlNi are present at 65.023° and 73.869°. The significant Al (111) and Ni (200) peaks are evaluated to assess the parent material presence. Diffractograms of Al$_{1.1}$Ni$_{0.9}$ and Al$_{0.42}$Ni$_{0.58}$ phase are very similar; therefore, they cannot be identified explicitly on the base of the measured XRD data. Consulting the EDX results and considering the fact, that fcc Ni is still present after RTA, it can be assumed, that Al$_{1.1}$Ni$_{0.9}$ (PDF 044-1187) is formed in this process, independently from surface modification and layer thickness. Peaks of fcc Ni were found on all black silicon samples in Figure 5 a). Its intensity decreases slightly with increasing T$_{max}$. This effect can be explained by emerging portions of the Ni-rich Al$_{0.42}$Ni$_{0.58}$ phase, which is formed at higher temperatures. Equally, it decreases on flat wafers with T$_{max}$ and here it disappears totally at T$_{max}$=550°C, compare Figure 5b). Strong Si peaks appear in this measurement due to regions where the reactive layer is peeled off. The samples annealed at 350°C show additional peaks, indicating the presence of Ni/Si phases. The intensity of the peaks related to Ni/Si phases disappear with increasing T$_{max}$.

The intensities of (111) Al peak, (200) Ni peak and (100) Al$_{1.1}$Ni$_{0.9}$ are used as markers to estimate the relation of present parent material and Al$_{1.1}$Ni$_{0.9}$ phase portions in the mixed crystal. The relative intensity I$_{relM}$ of the respective metal is calculated using Equation 1. The index M is representative of
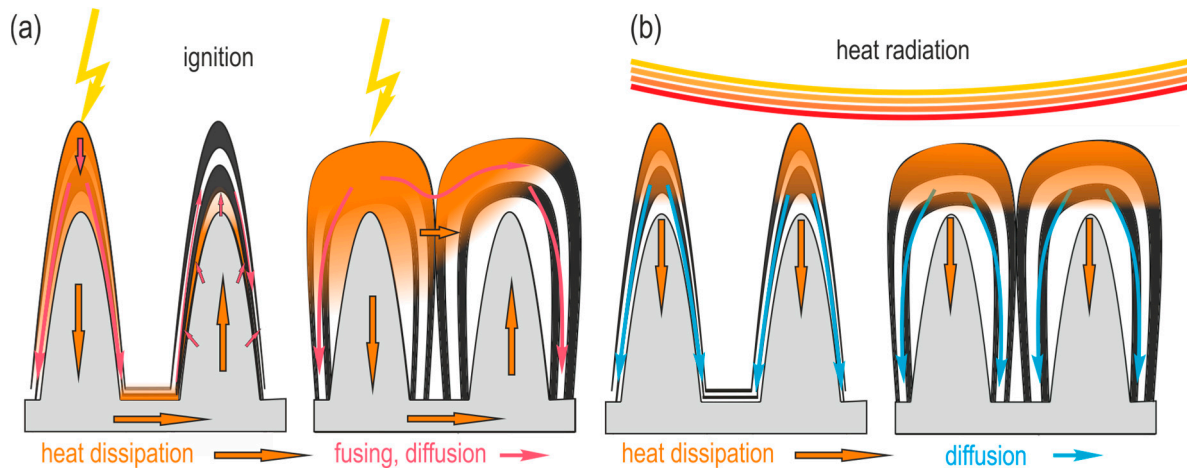
Figure 8.   Schematic illustration of the mass and heat transport for thin and thick multilayers. (a) Spark ignition; (b) Rapid thermal annealing.

199   the respective metal: Al= aluminum, Ni= nickel and AlNi= $Al_{1.1}Ni_{0.9}$ phase. The intensities I_{Al}, I_{Ni} and
200   I_{NiAl} are extracted from fitted curves of the respective measurement.

$$I_{relM} = \frac{I_M}{I_{Al}+I_{Ni}+I_{AlNi}} \times 100\% \qquad (1)$$

201   The obtained I_{relM} for all measurements carried out at 350°C are depicted in Figure 6. Figure 7
202   compares I_{relM} of the $Al_{1.1}Ni_{0.9}$ peak for multilayer thickness 1 µm and 5 µm with the values of 1-µm-
203   thick multilayer on the flat reference wafer.

204   **4. Discussion**

205   *4.1 Self-propagation of the reaction front*

206   Spark ignition creates a local hot spot, which heats a small region and initiates a chain reaction.
207   The propagation depends on amount of heat release and the level of heat losses to the environment.
208   It peters out when the balance of dissipated heat and reaction enthalpy, which is released during the
209   exothermic process, falls below the necessary activation energy. Figure 2 reveals molten areas around
210   the ignition points. Color changes identified by light microscope around the molten region indicate
211   a transition zone of the quenched reaction. The influenced area increases with layer thickness and
212   has a round shape as pointed out in Figure 2 a). An irregularity is observed on the samples with 1 µm
213   RML thickness. In this case, fused tips peter out astrally, which is visible in the SEM picture in Figure
214   2b). The self-propagating reaction spreads preferably along the tips of nanostructures with close
215   contact. Figure 8 a) illustrates the propagation process. The diffusion in thin layers must follow the
216   nanostructure contour, which enlarges the necessary diffusion path. The temperature at the ignition
217   point is high enough that the aluminum can melt and solid-liquid diffusion of Ni can occur. The fused
218   areas are visible in Figure 2 c-d). In parallel, high thermal conductivity of the silicon substrate causes
219   a rapid heat distribution. This can initiate additional solid-solid diffusion if the transformation
220   temperature is reached. This is assumed to be the reason for the formation of the transition zone.
221   Figure 2 e) depicts this transition zone for 500-nm-tick layer, which spreads over a length of 10 µm,
222   approximately. It seems that some separated nanostructures are molten form the bottom. The zone
223   observed on 5-µm-thick layers spans a dimension of 100 µm. This arise from the circumstance that
224   the larger reactive volume generates higher heat release whilst heat dissipation conditions are similar.
225   When the RML becomes thicker, the reaction wave starts to propagate along contact points at
226   the nanostructure tip. When the black silicon is covered with 1 µm thick RML layer, some structures
227   come into contact (compare Figure 1 d). The propagation along these contact points is the reason for
228   the irregular shape of the molten area occurring at this thickness (Figure 2 b). RML with a thickness
229   of 5 µm have a dense contact at the structure tip. This enables fusing along the layer top, enhancing
230   propagation. However, compared to RML deposited on flat surface, the affected radius is smaller
231   indicating that black silicon surface modification hinders the propagation.

232   The influence of grain boundary defects and the very low thickness of the RML at foot of black
233 silicon cannot clearly be judged. Some indications can be found in the literature: experiments reveal
234 that stacking faults and defects cause a decrease of the chain reaction efficiency if the bilayer thickness
235 fall below 20 nm [16]. A reduced cross section of the RML can hinder the propagation of the reaction
236 front and can be used to slow down the velocity [17], [18]. Molecular dynamic investigations suggest
237 that amorphous aluminum present at grain boundaries promotes the reaction [19]. The observation
238 in the present experiments suggest that the black silicon surface modification hinders the reaction.
239 Detailed investigations on atomic scale are needed to understand the complex process, when a
240 combustion waves propagate along curved structures with dimensions in the nanoscale.
241

242   *4.2 Rapid thermal annealing tests*

243   The dominant phase transformation mechanism during RTA is solid-state reaction, no molten
244 areas were observed on the samples. The heat radiation initiates the phase transformation at the
245 nanostructure tips and the transformation propagates perpendicular to the substrate plane, as
246 illustrated in Figure 8 b). Intermetallic phases around the stoichiometric AlNi composition are
247 formed. The $Al_{1.1}Ni_{0.9}$ phase contains 42-47 at% Ni [20]. Diffusion studies on Al-Ni-interfaces have
248 shown that the formation of intermetallic phases starts with Al-rich ones [21] as a consequence of the
249 lower melting point of the material. The sputtered parent RML contains stoichiometric composition
250 of Al and Ni. In RTA treated RML deposited on black silicon, fcc Ni still is present event at T_{max} of
251 550°C. The decreasing fcc Ni content with temperature is attributed to emerging Ni-rich intermetallic
252 phase, which requires higher temperatures [22]. The effect occurs similarly on flat samples, but here
253 the excessive fcc Ni already disappears at lower temperatures. A part of the excessive Ni forms a
254 material bound with the silicon substrate on flat surfaces (see Figure 5b). However, SiNi phases could
255 not be found on the nanostructured samples (Figure 5 a). This might be owed to the penetration depth
256 of the X-ray measurement, which might hinder the detection of occurring similar phases at the
257 nanostructured interface on the backside of the well adhered layers on these samples. A second
258 possibility is, that the nanostructure hinders the phase formation.
259   The comparison of the relative peak intensity I_{relM} in Figure 6 demonstrates that the annealing
260 temperature of 350°C is too low to achieve a complete transformation of RML on black silicon. The
261 remaining fcc Ni content increases with increasing RML thickness and fcc Al content remains stable
262 at the same time. This indicates that a complete transformation of the parent materials is not achieved
263 and Al-rich phase is formed preferably. The incompleteness of the transformation increases with
264 layer thickness, indicating that the annealing temperature of 350°C is too low to initiated an
265 exothermic chain reaction, because otherwise the released energy would foster a transformation. An
266 increase of the temperature up to 550°C (Figure 7) neither leads to a complete transformation. In
267 comparison to this, 1-μm-thick RML can be completely transformed at T_{max} 550°C if they are applied
268 on flat silicon. It can therefore be concluded that the nanostructured surface hinders the
269 transformation.

270 **5. Conclusions**

271   Reactive Al/Ni multilayer were deposited on nanostructured black silicon and pristine flat
272 silicon wafer for comparison purpose. The black silicon interface disturbs the morphology of the
273 parent AlNi multilayer, in particular at the foot of the nanostructure. In comparison with the flat
274 surface, black silicon hinders the self-propagating reaction initiated by electric spark. The solid-state
275 reaction initiated by rapid thermal annealing could not fully transform the parent materials on black
276 silicon, whilst it was achieved for flat surface at 550°C maximum temperature. The reaction is
277 hindered by the nanostructure as well. This behavior can help to control the reaction dynamics and it
278 can be used to control the reaction propagation when the RML is used for chip assembly on heat
279 sinks. The presence of almost stoichiometric AlNi phases leads to the conclusion, that high
280 temperatures have been achieved. Thus, the use of RML on black silicon as local heat source for
281 soldering processes with restricted heat-affected zone is possible.

The significantly enhanced adhesion of the RML on black silicon in comparison with the pristine wafer surface promises an additional improvement of the reliability of the thermal interface. Further studies must investigate stress, considering different chip assembly scenarios.

Since nanostructure influences microstructure of the parent material, reaction propagation and interface morphology, precise studies of single effects are necessary. As optimum way for understanding the complex process, a combination of molecular dynamic simulations and experimental work will be in the focus of pursuing works.

Acknowledgments: The authors acknowledge for the support from the Alexander von Humboldt Foundation, through the "Humboldt Research Fellowship for Postdoctoral Researchers Program" (Ref. 3.3-1 1S8421-ES-HFST-P). A special thank goes to Prof. Jens Müller for supervising this exchange. Further, the authors would express deep thankfulness to Prof. Peter Schaaf who enabled the sound cooperation among all staff of the material science department of IMN MacroNano® and the authors as base for this study.

Author Contributions: Heike Bartsch designed the experiments, performed the experiments, interpreted the results and wrote the paper. José Manuel Mánuel performed SEM and TEM studies, carried out XRD measurements and analyzed the respective data. Rolf Grieseler conceived the experiment and provided his experience of reactive multilayer processing and analysis. He supported the methodology concept and discussion section.

Conflicts of Interest: The authors declare no conflict of interest.

References

1. Grace O'Malley. *Highlights from the iNEMI Thermal Management Technology Roadmap*. *Advancing in manufacturing technology*, 2014. http://thor.inemi.org/webdownload/2014/Eurotherm_061914.pdf (accessed on 23 November 2017).

2. Yeh, L.-T. Thermal Management/Roadmap and Energy Efficiency for Telecommunications Equipment. *J Comput Intel Electron Syst* **2015**, *4*, 1–9, doi:10.1166/jcies.2015.1117.

3. Mahajan, R. *Thermal Interface Materials: A Brief Review of Design Characteristics and Materials*, February 1st, 2004. https://www.electronics-cooling.com/2004/02/thermal-interface-materials-a-brief-review-of-design-characteristics-and-materials/# (accessed on 28 November 2017).

4. Welker, T.; Geiling, T.; Bartsch, H.; Müller, J. Design and Fabrication of Transparent and Gas-Tight Optical Windows in Low-Temperature Co-Fired Ceramics. *Int. J. Appl. Ceram. Technol.* **2013**, *10*, 405–412, doi:10.1111/ijac.12034.

5. Subramanian, J.; Rodgers, P.; Newson, J.; Rude, T.R.; He, Z.; Besnoin, E.; Weihs, T.; Eveloy, V. Pecht,M. Room Temperature Soldering of Microelectronic Components for Enhanced Performance. In *International Conference on Thermal, Mechanical and Multiphysics Simulation and Experience in Microelectronics and Microsystems*; IEEE: Piscataway, 2005.

6. Bräuer, J.; Besser, J.; Wiemer, M.; Gessner, T. A novel technique for MEMS packaging: Reactive bonding with integrated material systems. *Sensors and Actuators A: Physical* **2012**, *188*, 212–219, doi:10.1016/j.sna.2012.01.015.

7. Bräuer, J.; Gessner, T. A hermetic and room-temperature wafer bonding technique based on integrated reactive multilayer systems. *J. Micromech. Microeng.* **2014**, *24*, 115002, doi:10.1088/0960-1317/24/11/115002.

8. Grieseler, R.; Welker, T.; Müller, J.; Schaaf, P. Bonding of low temperature co-fired ceramics to copper and to ceramic blocks by reactive aluminum/nickel multilayers. P*hysica status solidi (a)* **2012**, *209, doi:*10.1002/pssa.201127470.

9. Miyake, S.; Kanetsuki, S.; Morino, K.; Kuroishi, J.; Namazu, T. Thermal property measurement of solder joints fabricated by self-propagating exothermic reaction in Al/Ni multilayer film. *Jpn. J. Appl. Phys.* **2015**, *54*, 06FP15, doi:10.7567/JJAP.54.06FP15.

10. Namazu, T.; Ohtani, K.; Inoue, S.; Miyake, S. Influences of Exothermic Reactive Layer and Metal Interlayer on Fracture Behavior of Reactively Bonded Solder Joints. *J. Eng. Mater. Technol.* **2015**, *137*, 31011, doi:10.1115/1.4030413.

11. Bar-Cohen, A.; Matin, K.; Narumanchi, S. Nanothermal Interface Materials: Technology Review and Recent Results. *Journal of Electronic Packaging* **2015**, *137*, 40803, doi:10.1115/1.4031602.

12. Feng, B.; Cao, J.; Wang, Y.; Feng, J. Enhanced Adhesive Bonding Based on Surface Modification with Silicon Nanowire Arrays. *ECS J. Solid State Sci. Technol.* **2015**, *5*, P41-P46, doi:10.1149/2.0141602jss.

334   13.   Fischer, M.; Bartsch, H.; Pawlowski, B.; Gade, R.; Barth, S.; Mach, M.; Stubenrauch, M.; Hoffmann, M.;
335   Müller, J. Silicon on Ceramics - A New Integration Concept for Silicon Devices to LTCC. *Journal of*
336   *microelectronics and electronic packaging* **2009**, 1–5.
337   14.   Jansen, H.V.; Boer, M.J. de; Unnikrishnan, S.; Louwerse, M.C.; Elwenspoek, M.C. Black silicon method: X.
338   A review on high speed and selective plasma etching of silicon with profile control: an in-depth comparison
339   between Bosch and cryostat DRIE processes as a roadmap to next generation equipment. *J. Micromech.*
340   *Microeng.* **2009**, *19*, 33001, doi:10.1088/0960-1317/19/3/033001.
341   15.   Pezoldt, J.; Kups, T.; Stubenrauch, M.; Fischer, M. Black luminescent silicon. *Phys. Status Solidi (c)* **2011**, *8*,
342   1021–1026, doi:10.1002/pssc.201000388.
343   16.   Theodossiadis, G.D.; Zaeh, M.F. Study of the kinetic and energetic reaction properties of multilayered
344   aluminum–nickel nanofoils. *Prod. Eng. Res. Devel.* **2017**, *11*, 245–253, doi:10.1007/s11740-017-0733-8.
345   17.   Sraj, I.; Vohra, M.; Alawieh, L.; Weihs, T.P.; Knio, O.M. Self-Propagating Reactive Fronts in Compacts of
346   Multilayered Particles. *Journal of Nanomaterials* **2013**, *2013*, 1–11, doi:10.1155/2013/198096.
347   18.   Fritz, G.M.; Joress, H.; Weihs, T. Enabling and controlling slow reaction velocities in low-density compacts
348   of multilayer reactive particle. *Combustion and Flame* **2011**, *158*, 1084–1088.
349   19.   Politano, O.; Baras, F.; Mukasyan, A.S.; Vadchenko, S.G.; Rogachev, A.S. Microstructure development
350   during NiAl intermetallic synthesis in reactive Ni–Al nanolayers: Numerical investigations vs. TEM
351   observations. *Surface and Coatings Technology* **2013**, *215*, 485–492, doi:10.1016/j.surfcoat.2012.09.065.
352   20.   Urrutia, A.; Tumminello, S.; Aricó, S.F.; Sommadossi, S. Characterization of Al–Ni intermetallics around
353   30–60at% Al for TLPB application. *Calphad* **2014**, *44*, 108–113, doi:10.1016/j.calphad.2013.08.004.
354   21.   Tumminello, S.; Sommadossi, S. Growth Kinetics of Intermetallic Phases in Transient Liquid Phase Bonding
355   Process (TLPB) in Al /Ni System. *DDF* **2012**, *323-325*, 465–470, doi:10.4028/www.scientific.net/DDF.323-
356   325.465.
357   22.   Urrutia, A.; Tumminello, S.; Lamas, D.G.; Sommadossi, S. X-Ray Characterization of Intermetallic Phases
358   in Al/Ni Multilayer System. *Procedia Materials Science* **2015**, *8*, 1150–1159, doi:10.1016/j.mspro.2015.04.179.